



## Capturing coastal water clarity variability with Landsat 8

Kelly M.A. Luis<sup>a,\*</sup>, Jennie E. Rheuban<sup>b</sup>, Maria T. Kavanaugh<sup>c</sup>, David M. Glover<sup>b</sup>, Jianwei Wei<sup>a</sup>, Zhongping Lee<sup>a</sup>, Scott C. Doney<sup>b,d</sup>

<sup>a</sup> School for the Environment, University of Massachusetts Boston, Boston, MA, USA

<sup>b</sup> Department of Marine Chemistry and Geochemistry, Woods Hole Oceanographic Institution, Woods Hole, MA 02543, USA

<sup>c</sup> College of Earth, Ocean, and Atmospheric Sciences, Oregon State University, Corvallis, OR 97330, USA

<sup>d</sup> Department of Environmental Sciences, University of Virginia, Charlottesville, VA 22904, USA

### ARTICLE INFO

#### Keywords:

Water quality  
Secchi disk depth  
Remote sensing  
Landsat

### ABSTRACT

Coastal water clarity varies at high temporal and spatial scales due to weather, climate, and human activity along coastlines. Systematic observations are crucial to assessing the impact of water clarity change on aquatic habitats. In this study, Secchi disk depths ( $Z_{SD}$ ) from Boston Harbor, Buzzards Bay, Cape Cod Bay, and Narragansett Bay water quality monitoring organizations were compiled to validate  $Z_{SD}$  derived from Landsat 8 (L8) imagery, and to generate high spatial resolution  $Z_{SD}$  maps. From 58 L8 images, acceptable agreement was found between in situ and L8  $Z_{SD}$  in Buzzards Bay ( $N = 42$ ,  $RMSE = 0.96$  m,  $MAPD = 28\%$ ), Cape Cod Bay ( $N = 11$ ,  $RMSE = 0.62$  m,  $MAPD = 10\%$ ), and Narragansett Bay ( $N = 8$ ,  $RMSE = 0.59$  m,  $MAPD = 26\%$ ). This work demonstrates the value of merging in situ  $Z_{SD}$  with high spatial resolution remote sensing estimates for improved coastal water quality monitoring.

### 1. Introduction

Coastal ecosystems require systematic observations to document spatio-temporal changes in water clarity, a good indicator for overall water quality. Temporal variations can occur on hourly timescales due to diel and tidal cycles and spatial variations can occur on an order of tens of meters due to fluctuating weather and climate patterns and increasing human activity along coastlines. In situ water clarity measurements such as Secchi disk depths ( $Z_{SD}$ ) and turbidity from water quality monitoring organizations provide detailed and accurate observations but tend to be limited by spatial and temporal coverage due to cost and logistical challenges. Satellite remote sensing can be used to fill these spatial and temporal sampling gaps.

Traditional ocean color satellite sensors, such as Moderate Resolution Imaging Spectrometer (MODIS) or Medium Resolution Imaging Spectrometer (MERIS), are generally designed for open ocean systems; as a result, the spatial resolution of these sensors is too coarse (~300–1000 m) to capture dynamic coastal processes. Landsat, a satellite series primarily designed for observing terrestrial targets, has a spatial resolution of 30 m, which allows for synoptic observations in small lakes, bays, and harbors that traditional ocean color sensors cannot resolve. For instance, turbidity change, black water events, and phytoplankton blooms in Florida Bay (FL, USA) were detected with

Landsat imagery (Barnes et al., 2014). Landsat imagery has also been analyzed to map turbidity and sediment plumes across New York Harbor (NY, USA) (Hellweger et al., 2004). The application of Landsat imagery to inland, estuarine, and coastal waters has resulted in the development of water quality algorithms aimed at obtaining quantitative biogeochemical information such as chlorophyll, colored dissolved organic matter, suspended particulate matter, and water clarity (Lim and Choi, 2015; Olmanson et al., 2016; Sun et al., 2015; Trinh et al., 2017).

Although underlying drivers of water quality cannot be determined from clarity alone, water clarity is a good indicator of overall water quality and can be determined easily by a Secchi disk, a 30 cm in diameter white, or black-and-white, disk. An individual measures water clarity with a Secchi disk by lowering the disk into the water, and the depth at which the disk is no longer visible from the surface is the Secchi disk depth ( $Z_{SD}$ ).  $Z_{SD}$  is determined by the amount of optically variable constituents (i.e. phytoplankton, detritus, colored dissolved organic matter, inorganic particles) in the water column (Preisendorfer, 1986; Wernand, 2010). Despite the increasing sophistication of bio-optical sensors for water clarity measurements, Secchi disks are still widely used because of its ease of use and low cost (Aas et al., 2014; Boyce et al., 2012; Wernand, 2010).

Remote sensing estimates of water clarity are typically derived

\* Corresponding author.

E-mail address: [kelly.luis001@umb.edu](mailto:kelly.luis001@umb.edu) (K.M.A. Luis).

<https://doi.org/10.1016/j.marpolbul.2019.04.078>

Received 22 December 2018; Received in revised form 29 April 2019; Accepted 30 April 2019

0025-326X/ © 2019 The Authors. Published by Elsevier Ltd. This is an open access article under the CC BY license (<http://creativecommons.org/licenses/by-nc-nd/4.0/>).

empirically (Crooke et al., 2017; Doron et al., 2011; Kloiber et al., 2002). However, the application of empirical algorithms is limited to water types with similar optically variable constituents because the algorithm coefficients depend on the datasets used during the algorithm development. Locally validated radiative transfer-based algorithms are necessary for the application to a range of water types (Chen et al., 2007; Doron et al., 2007; Weeks et al., 2012), which is critical for coastal water bodies where the constituents vary widely.

To understand  $Z_{SD}$  and its derivation from remote sensing, Lee et al. (2015) reevaluated classical theoretical interpretations of  $Z_{SD}$  (Duntley and Preisendorfer, 1952; Preisendorfer, 1986) and proposed a new underwater visibility model that inversely relates  $Z_{SD}$  to the diffuse attenuation coefficient at the wavelength of maximum light penetration. The Lee et al. (2015) model was validated with in situ measurements from oceanic, coastal, and inland waters, where in situ and derived  $Z_{SD}$  agreed well ( $\sim 18\%$  absolute difference,  $R^2 = 0.96$ ,  $N = 338$ ). The Lee et al. (2015)  $Z_{SD}$  model was parameterized for Landsat 8 (L8) imagery and applied to the Jiulong River, China (Lee et al., 2016). The performance of the Lee et al. (2016) L8  $Z_{SD}$  algorithm was further evaluated in the Nav reservoir, an oligotrophic-mesotrophic inland water body in Sao Paulo, Brazil (Rodrigues et al., 2017). The atmospheric correction methods and the derivation of inherent optical properties (IOP) from L8 data were observed to limit the accuracy of the L8  $Z_{SD}$  algorithm. By recalibrating the derivation of IOPs, Rodrigues et al. (2017) found the  $Z_{SD}$  algorithm applicable to the Nav Reservoir. However, a robust validation and application of the L8  $Z_{SD}$  algorithm to a range of coastal water bodies has yet to be conducted.

Thus, we applied the Lee et al. (2016) L8  $Z_{SD}$  algorithm to four coastal water bodies (Fig. 1): Boston Harbor (USA; 42.34° N, 70.96° W), Buzzards Bay (USA; 41.55° N, 70.80° W), Cape Cod Bay (USA; 41.85° N, 70.34° W), and Narragansett Bay (USA; 41.62° N, 71.35° W). The variations in seasonality and bathymetry observed within the same L8 image make these regions ideal locations for evaluating the precision of the L8  $Z_{SD}$  algorithm across different environmental conditions. More

importantly, these water bodies are routinely monitored by water quality monitoring organizations dedicated to preserving the environmental, economic, and recreational vitality of these water bodies. In situ  $Z_{SD}$  measurements from local scientists and citizen scientists were compiled to validate the L8  $Z_{SD}$  measurements. This analysis ultimately demonstrates the validation and application of the L8 water clarity algorithm to a range of coastal water bodies and highlights L8 imagery's ability to broaden our understanding of spatio-temporal coastal water clarity variations.

## 2. Data and methods

### 2.1. In situ $Z_{SD}$ measurements

In situ measurements of  $Z_{SD}$  were collected from water quality monitoring programs in Boston Harbor, Buzzards Bay, Cape Cod Bay, and Narragansett Bay. Boston Harbor is a tidally dominated estuary (130 km<sup>2</sup>) on the western edge of Massachusetts Bay. The Massachusetts Water Resources Authority has monitored Boston Harbor's water quality since 1994. Buzzards Bay is a long, shallow estuary (600 km<sup>2</sup>) bordered by southeastern Massachusetts, Cape Cod, and the Elizabeth Islands that has been monitored every summer since 1992 by Buzzards Bay Coalition's citizen scientists. Cape Cod Bay is a large, semi-enclosed bay (1560 km<sup>2</sup>) on the southern edge of Massachusetts Bay and bounded to the south by Cape Cod and has been monitored by citizen scientists throughout the year with the Provincetown Center for Coastal Studies since 2002. Narragansett Bay is a partially mixed estuary (342 km<sup>2</sup>) north of Block Island Sound. The Environmental Monitoring and Data Analysis section of the Narragansett Bay Commission has monitored Narragansett Bay's water quality since 2001. In this study, water clarity stations from Upper Narragansett Bay were assessed.  $Z_{SD}$  from Boston Harbor, Buzzards Bay, and Cape Cod Bay were measured similarly, where the  $Z_{SD}$  was recorded as the depth the Secchi disk is no longer visible by an individual

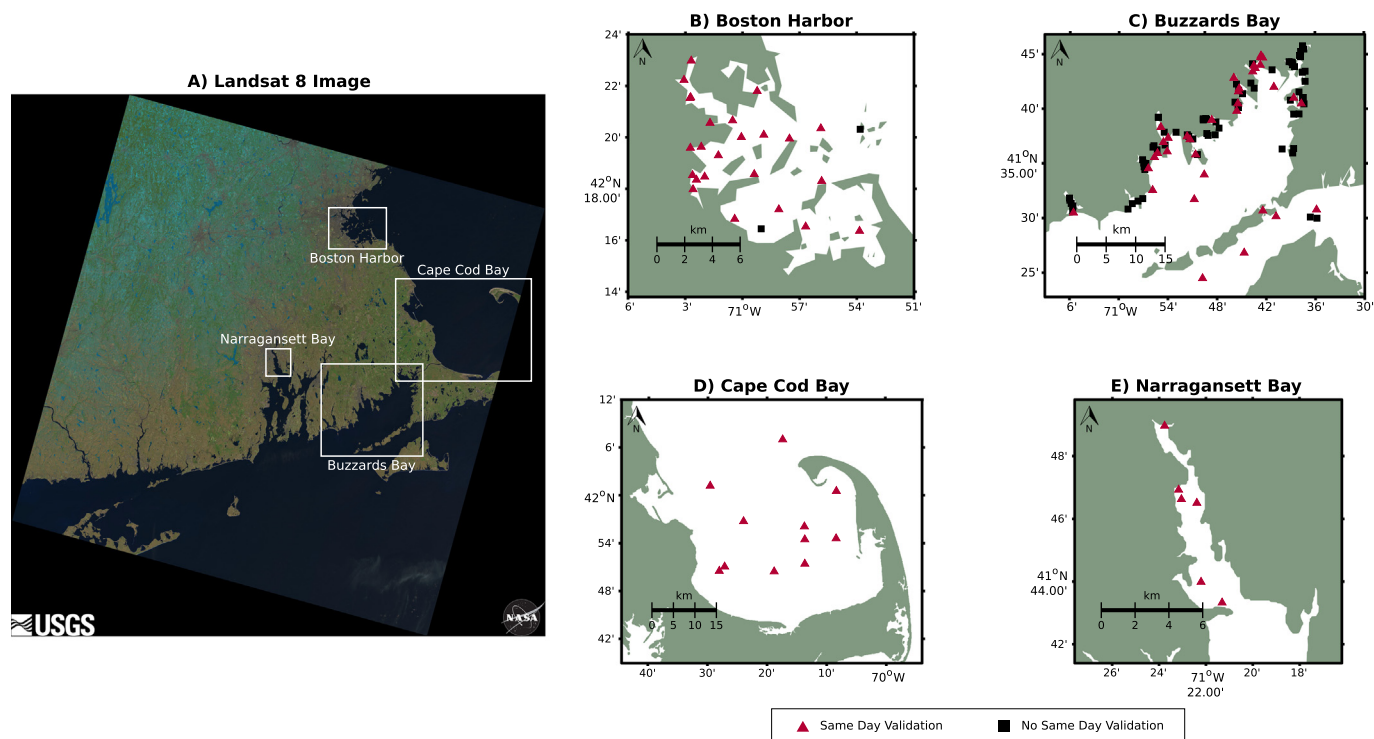


**Fig. 1.** Locations of in situ and L8  $Z_{SD}$  measurements. Red triangles represent sites with same day in situ  $Z_{SD}$  measurements and black squares represent sites without same day in situ  $Z_{SD}$  measurements A) Landsat 8 image from March 14, 2014 B) Boston Harbor (MA, USA) C) Buzzards Bay (MA, USA) D) Cape Cod Bay (MA, USA) E) Narragansett Bay (RI, USA). (For interpretation of the references to color in this figure legend, the reader is referred to the web version of this article.)

**Table 1**  
List of Landsat 8 images analyzed.

Image name	Date
LC08_L1TP_012031_20130404_20170310_01_T1	4-Apr-13
LC08_L1TP_012031_20130409_20170310_01_T1	9-Apr-13
LC08_L1TP_012031_20130416_20170310_01_T1	16-Apr-13
LC08_L1TP_012031_20130502_20170310_01_T1	2-May-13
LC08_L1TP_012031_20130518_20170310_01_T1	18-May-13
LC08_L1TP_012031_20130619_20170309_01_T1	19-Jun-13
LC08_L1TP_012031_20130705_20170309_01_T1	5-Jul-13
LC08_L1TP_012031_20130806_20170309_01_T1	6-Aug-13
LC08_L1TP_012031_20130822_20170309_01_T1	22-Aug-13
LC08_L1TP_012031_20130907_20170309_01_T1	7-Sep-13
LC08_L1TP_012031_20130923_20170308_01_T1	23-Sep-13
LC08_L1TP_012031_20131212_20170307_01_T1	12-Dec-13
LC08_L1TP_012031_20140113_20170306_01_T1	13-Jan-14
LC08_L1TP_012031_20140318_20170306_01_T1	18-Mar-14
LC08_L1TP_012031_20140403_20170307_01_T1	3-Apr-14
LC08_L1TP_012031_20140419_20170307_01_T1	19-Apr-14
LC08_L1TP_012031_20140521_20170307_01_T1	21-May-14
LC08_L1TP_012031_20140606_20170305_01_T1	6-Jun-14
LC08_L1TP_012031_20140622_20170304_01_T1	22-Jun-14
LC08_L1TP_012031_20140809_20170304_01_T1	9-Aug-14
LC08_L1TP_012031_20141129_20170302_01_T1	29-Nov-14
LC08_L1TP_012031_20141215_20170302_01_T1	15-Dec-14
LC08_L1TP_012031_20141231_20170302_01_T1	31-Dec-14
LC08_L1TP_012031_20150116_20170302_01_T1	16-Jan-15
LC08_L1TP_012031_20150201_20170301_01_T1	1-Feb-15
LC08_L1TP_012031_20150422_20170301_01_T1	22-Apr-15
LC08_L1TP_012031_20150508_20170227_01_T1	8-May-15
LC08_L1TP_012031_20150524_20170226_01_T1	24-May-15
LC08_L1TP_012031_20150625_20170226_01_T1	25-Jun-15
LC08_L1TP_012031_20150711_20170226_01_T1	11-Jul-15
LC08_L1TP_012031_20150812_20170226_01_T1	12-Aug-15
LC08_L1TP_012031_20150828_20170225_01_T1	28-Aug-15
LC08_L1TP_012031_20151015_20170225_01_T1	15-Oct-15
LC08_L1TP_012031_20151031_20170225_01_T1	31-Oct-15
LC08_L1TP_012031_20151116_20170225_01_T1	15-Nov-15
LC08_L1TP_012031_20160103_20170224_01_T1	3-Jan-16
LC08_L1TP_012031_20160119_20170224_01_T1	19-Jan-16
LC08_L1TP_012031_20160220_20170224_01_T1	20-Feb-16
LC08_L1TP_012031_20160408_20170223_01_T1	8-Apr-16
LC08_L1TP_012031_20160424_20170223_01_T1	24-Apr-16
LC08_L1TP_012031_20160510_20170223_01_T1	10-May-16
LC08_L1TP_012031_20160526_20170223_01_T1	26-May-16
LC08_L1TP_012031_20160627_20170223_01_T1	27-Jun-16
LC08_L1TP_012031_20160713_20180130_01_T1	13-Jul-16
LC08_L1TP_012031_20160814_20170221_01_T1	14-Aug-16
LC08_L1TP_012031_20160830_20180130_01_T1	30-Aug-16
LC08_L1TP_012031_20160915_20170223_01_T1	15-Sep-16
LC08_L1TP_012031_20161017_20170219_01_T1	17-Oct-16
LC08_L1TP_012031_20161102_20170221_01_T1	2-Nov-16
LC08_L1TP_012031_20161118_20180130_01_T1	18-Nov-16
LC08_L1TP_012031_20170614_20170628_01_T1	14-Jun-17
LC08_L1TP_012031_20170716_20170727_01_T1	16-Jul-17
LC08_L1TP_012031_20170801_20170811_01_T1	1-Aug-17
LC08_L1TP_012031_20170817_20170826_01_T1	17-Aug-17
LC08_L1TP_012031_20171004_20171014_01_T1	4-Oct-17
LC08_L1TP_012031_20171020_20171106_01_T1	20-Oct-17
LC08_L1TP_012031_20171121_20171206_01_T1	21-Nov-17
LC08_L1TP_012031_20171207_20180125_01_T1	7-Dec-17

from the surface. Narragansett Bay  $Z_{SD}$  resulted from the average of two depth measurements: 1) depth the disk is no longer visible from the surface, 2) depth just before the disk disappears. In this study, we included in situ  $Z_{SD}$  beginning in April 2013 until December 2017 to correspond with L8's measurements.

## 2.2. Satellite data

A total of 58 clear sky L8 images from April 2013 through December 2017 (Table 1) were retrieved from Earth Explorer (<https://earthexplorer.usgs.gov/>). The Level-1 images were processed with SeaDAS (<https://seadas.gsfc.nasa.gov/>) to generate remote sensing

reflectance ( $R_{rs}$ ,  $sr^{-1}$ ). The NASA standard NIR-SWIR algorithm was used for atmospheric correction. Specifically, bands 5 and 7 (865 nm and 2201 nm, respectively) were used in current study; this band combination yields higher quality  $R_{rs}$  products in nearshore waters (Wei et al., 2018). The standard Level-2 quality flags were masked, including ATMFAIL (atmospheric correction failure), LAND (land pixel), CLDICE (probable cloud or ice contamination) and HILT (very high or saturated radiance). The  $R_{rs}$  products were further processed with the Quasi-Analytical Algorithm (QAA, <http://www.ioccc.org/groups/software.html>) to derive the total absorption,  $a$ , and backscattering,  $b_b$ , coefficients (Lee et al., 2002, 2016), which are the inputs for deriving the diffuse attenuation coefficient,  $K_d$  ( $m^{-1}$ ), with Lee et al. (2013)  $K_d$  model.

## 2.3. L8 $Z_{SD}$ algorithm

The classical underwater visibility theory interpreted the Secchi disk depth ( $Z_{SD}$ ) as inversely proportional to the sum of the diffuse attenuation coefficient,  $K_d$  ( $m^{-1}$ ), and the beam attenuation,  $c$  ( $1/m$ ), within the visible domain (Preisendorfer, 1986). However, Lee et al. (2015, 2016) argued that  $Z_{SD}$  is related to  $K_d$  in the transparent window, with  $Z_{SD}$  expressed as:

$$Z_{SD} = \frac{1}{2.5(K_d^r)} \ln \left| \frac{0.14 - R_{rs}^r}{0.013} \right| \quad (1)$$

where  $K_d^r$  represents the minimum diffuse attenuation coefficient of a water body over the visible domain (400–700 nm) and  $R_{rs}^r$  the corresponding remote-sensing reflectance at this wavelength.

As described in Lee et al. (2005, 2015, 2016)  $K_d$  can be analytically derived from a multi-spectral or hyperspectral  $R_{rs}$  spectrum. Thus,  $K_d^r$  can be easily determined if the input  $R_{rs}$  has numerous spectral bands in the visible domain, which is not the case for L8 because it only has four spectral bands (443, 482, 561, and 670 nm) in the visible range. To fill the wide spectral gap between 482 nm and 561 nm, Lee et al. (2016) developed an empirical relationship to estimate the diffuse attenuation coefficient at 530 nm ( $K_d(530)$ ). The addition of  $K_d(530)$  improves the determination of a minimum  $K_d$  in the visible domain ( $K_d^r$ ). Subsequently,  $Z_{SD}$  can be calculated following Eq. (1) from L8  $R_{rs}$  as described in detail in Lee et al. (2016).

## 2.4. Validation

The accuracy of the L8  $Z_{SD}$  estimate was evaluated with same-day in situ  $Z_{SD}$  matchup values (Fig. 2),  $Z_{SD}$  range and distribution variability (Fig. 3), and seasonal variations in  $Z_{SD}$  from 2013 to 2017 (Fig. 4). The L8  $Z_{SD}$  values in Figs. 2, 3, and 4 represent the mean and standard deviation of  $Z_{SD}$  values in a  $3 \times 3$  pixel ( $90 \times 90$  m) box centered at the coordinates of in situ stations. In situ  $Z_{SD}$  measurements on the same day of the L8 overpass were used to validate the L8  $Z_{SD}$  algorithm with results presented in Fig. 2. Optically shallow sites, where a  $Z_{SD}$  was not recorded because the bottom was visible from the surface by an observer, were excluded from the validation. Root mean square error (RMSE) and mean absolute percentage difference (MAPD) were used to gauge the consistency of the same day matchup:

$$RMSE = \sqrt{\frac{1}{n} \sum_{i=1}^n (x_{derived,i} - x_{in situ,i})^2} \quad (2)$$

$$MAPD = \frac{1}{n} \sum_{i=1}^n \left| \frac{x_{derived,i} - x_{in situ,i}}{x_{in situ,i}} \right| \times 100\% \quad (3)$$

The L8  $Z_{SD}$  range and distribution variability were evaluated in Fig. 3 with histograms and box plots. In situ  $Z_{SD}$  within an atmospherically corrected pixel and within the same month and year of an L8 overpass were included in this study. For L8  $Z_{SD}$ , L8 pixels that contained corresponding station coordinates from water quality

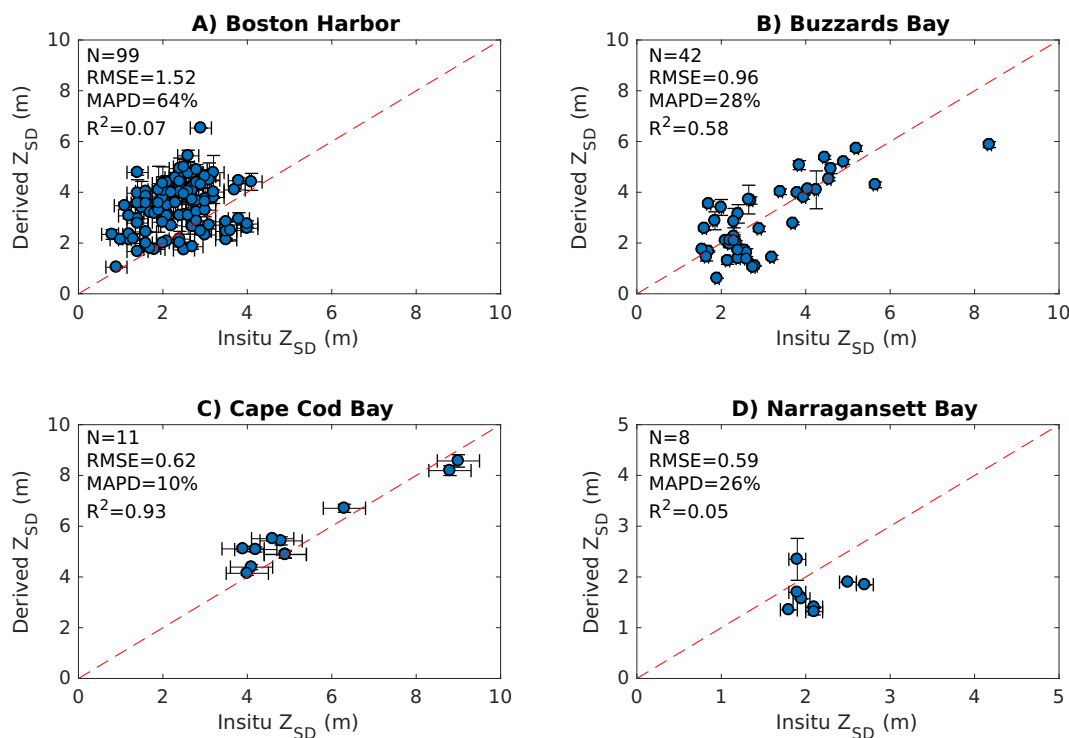


**Fig. 2.** Same day in situ and L8  $Z_{SD}$  matchup: A) Boston Harbor, B) Buzzards Bay, C) Cape Cod Bay, D) Narragansett Bay. In situ  $Z_{SD}$  error bars accounts for the error associated with the  $Z_{SD}$  tape markings and L8  $Z_{SD}$  error bars represents the standard deviation of the  $3 \times 3$  L8 pixels.

monitoring organizations were included. As a result, 26 of Boston Harbor sites, 106 of Buzzards Bay sites, 11 of Cape Cod Bay sites, and 7 of Narragansett Bay sites were included in this assessment. The box-whisker plots display the following summary statistics: mean, median, interquartile range, and 9% and 91% quantiles.

Lastly, in situ and L8  $Z_{SD}$  were compared across 2013–2017 to determine how well L8  $Z_{SD}$  captured seasonal variations in water clarity (Fig. 4). In situ chlorophyll, pheophytin, total suspended solids, attenuation, and turbidity seasonal trends were also compared with  $Z_{SD}$  for Boston Harbor, Cape Cod Bay, and Narragansett Bay (Supplementary figures). It is important to note that for both range and variability validation (Fig. 3) and the seasonal validation (Fig. 4) the dates of the L8 overpasses and the in situ measurements do not match precisely; nevertheless, the analyses provided important information about spatio-temporal variations based on a larger set of in situ and L8  $Z_{SD}$  measurements than is available for same-day validation.

### 3. Results

#### 3.1. Same-day in situ $Z_{SD}$ and L8 $Z_{SD}$

Of the 58 L8 clear sky images, 14 images occurred on the same day of Boston Harbor sampling dates, 15 images occurred on the same day of Buzzards Bay water quality sampling dates, 1 image occurred on the same day of the Cape Cod Bay water quality sampling dates, and 3 images occurred on the same day of Narragansett Bay water quality sampling dates (see Fig. 1). Observed values varied substantially for both chlorophyll (0.38–68.9 mg/m<sup>3</sup>) and turbidity (0.1–77.4 NTU). Yet despite the differences in the underlying water body, time of year, and in situ observations by different observers, there was good agreement between the two independent determinations (in situ vs L8) for Buzzards Bay ( $N = 42$ ,  $RMSE = 0.96$  m,  $MAPD = 28\%$ ,  $R^2 = 0.58$ ), Cape Cod Bay ( $N = 11$ ,  $RMSE = 0.62$  m,  $MAPD = 10\%$ ,  $R^2 = 0.93$ ), and Narragansett Bay ( $N = 8$ ,  $RMSE = 0.59$  m,  $MAPD = 36\%$ ,  $R^2 = 0.05$ ) (Fig. 2). To increase the number of observations for Narragansett Bay's validation, the degree of autocorrelation for high frequency chlorophyll

fluorometer measurements was analyzed to inform the expansion of the temporal validation window. While chlorophyll is not the sole driver of water clarity, chlorophyll was the only long-term, high frequency optically variable constituent available and still provided insight about Narragansett Bay's temporal water clarity variability. Since chlorophyll measurements became decorrelated after two days, the validation window was increased to two days and the in situ and L8  $Z_{SD}$  were still in good agreement ( $N = 35$ ,  $RMSE = 0.69$  m,  $MAPD = 34\%$ ,  $R^2 = 0.08$ ).

Unlike Narragansett Bay, poor same-day agreement between Boston Harbor's in situ  $Z_{SD}$  and L8  $Z_{SD}$  ( $N = 99$ ,  $RMSE = 1.52$  m,  $MAPD = 64\%$ ,  $R^2 = 0.07$ ) was found. When Boston Harbor's temporal window was limited to 3 h of L8 overpasses, in situ and L8  $Z_{SD}$  matchup improved, but the agreement was still poor ( $N = 20$ ,  $RMSE = 1.3$  m,  $MAPD = 50\%$ ,  $R^2 = 0.11$ ). To minimize contamination from adjacent land pixels, Boston Harbor's nearshore stations (within 90 m  $\sim 3$  L8 pixels away from the nearest coastline) were excluded from the three-hour validation window and the in situ and L8  $Z_{SD}$  matchup improved slightly ( $N = 9$ ,  $RMSE = 1.26$  m,  $MAPD = 45\%$ ,  $R^2 = 0.14$ ).

#### 3.2. $Z_{SD}$ range variability

L8  $Z_{SD}$  values captured the range and distribution of water clarity observed across Boston Harbor, Buzzards Bay, Cape Cod Bay, and Narragansett Bay (Fig. 3). Boston Harbor, Buzzards Bay, and Narragansett Bay's in situ and L8  $Z_{SD}$  ranged from 1 to 5 m and the majority of the measurements clustered around 2–3 m, which is characteristic of the small harbors, inlets, and embayments in these three water bodies. The in situ and L8  $Z_{SD}$  in Cape Cod Bay ranged from 4 to 10 m and the majority of the measurements clustered around 5–6 m, which is characteristic of the Cape Cod Bay stations used in this study.

Histograms for Buzzards Bay and Narragansett Bay were positively skewed indicating a few of the in situ and L8  $Z_{SD}$  were high ( $> 6$  m), but the majority of in situ and L8  $Z_{SD}$  were clustered around lower  $Z_{SD}$  values ( $< 3$  m). The overlapping in situ and L8 interquartile ranges for Buzzards Bay (2–3 m) and Narragansett Bay (2–3 m) indicated that the

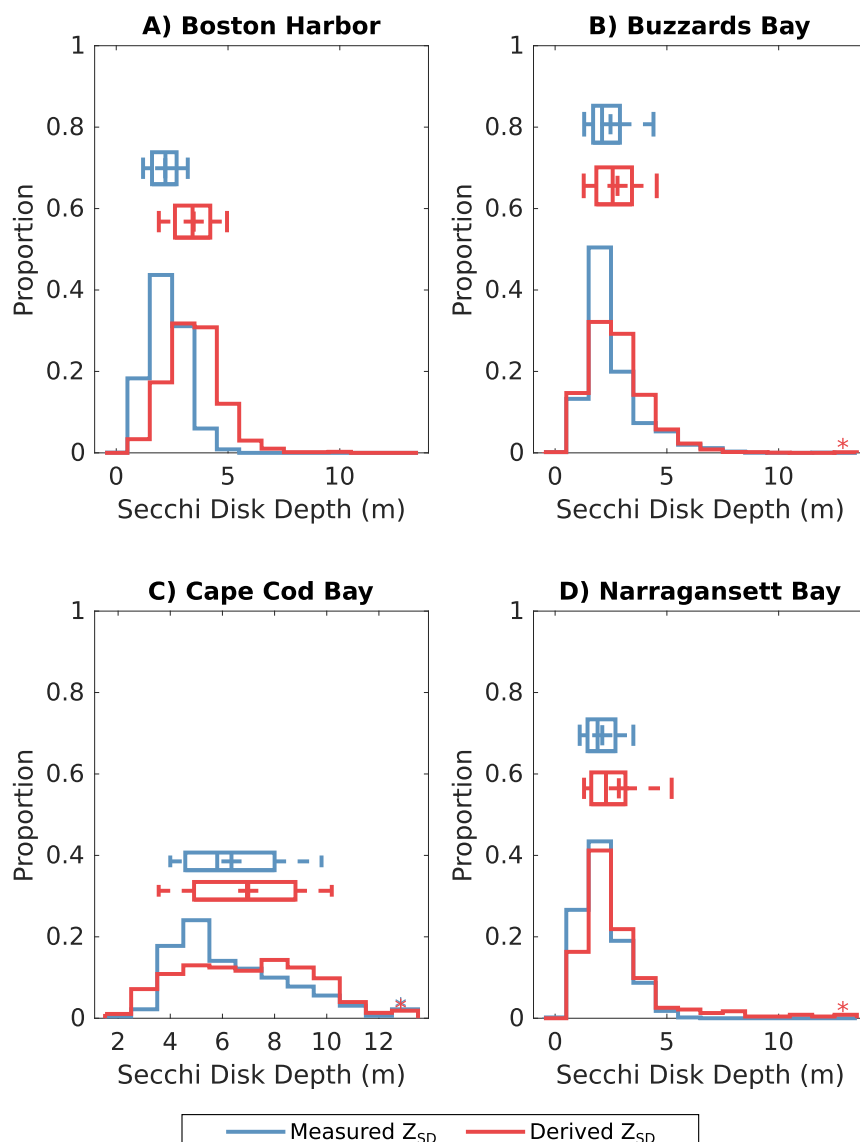


**Fig. 3.** Histograms and boxplots of the range and distribution of in situ and L8  $Z_{SD}$  from all 58 L8 images: A) Boston Harbor, B) Buzzards Bay, C) Cape Cod Bay, D) Narragansett Bay.

L8  $Z_{SD}$  captured the overall characteristics of the in situ  $Z_{SD}$ . Cape Cod Bay's  $Z_{SD}$  distribution spread was similar to Buzzards Bay and Narragansett Bay where the interquartile ranges (5–8 m) overlapped and the in situ and L8  $Z_{SD}$  distributions were positively skewed. For Boston Harbor, the in situ and L8  $Z_{SD}$  distributions were more symmetric where the mean and median are similar, but the L8  $Z_{SD}$  mean and median were greater than the in situ  $Z_{SD}$  by 1 m, which was consistent with the same-day validation results (Fig. 2) where L8  $Z_{SD}$  generally overpredicted the in situ  $Z_{SD}$  by over a meter. In addition, the interquartile range for the L8  $Z_{SD}$  shifted to the right of the in situ  $Z_{SD}$  by a meter, which further indicates the overprediction of L8  $Z_{SD}$  in Boston Harbor.

### 3.3. $Z_{SD}$ temporal assessment

Although we analyzed all sites observed by citizen scientists and L8, for simplicity, we present one site from each water body to exhibit the temporal variability of in situ and L8  $Z_{SD}$  (Fig. 4). The in situ and L8  $Z_{SD}$  at site 142 in Boston Harbor, located between Boston Harbor Islands' Deer Island and Lovell's Island, had comparable  $Z_{SD}$  ranges (in situ  $Z_{SD}$ : 1–5 m and L8  $Z_{SD}$ : 2–6 m) throughout 2013–2017, and exhibited no

distinctive seasonal trends; although, the L8  $Z_{SD}$  appeared consistently deeper than in situ  $Z_{SD}$ . Additionally, coinciding chlorophyll, pheophytin, attenuation, total suspended solids, and turbidity measurements in Boston Harbor exhibited no seasonal trends (S1), a similar temporal pattern exhibited by  $Z_{SD}$ .

While the Buzzards Bay in situ and L8  $Z_{SD}$  exhibited the same range, since Buzzards Bay sampling only occurred in the summer months, we were unable to determine if in situ and L8  $Z_{SD}$  had the same seasonal cycle. Interestingly, from 2013 to 2017, L8  $Z_{SD}$  values from Buzzards Bay were the lowest during the winter months (December–February) and highest during the spring months (March–May). A similar  $Z_{SD}$  pattern was observed in Cape Cod Bay where low  $Z_{SD}$  were found in the winter and early spring months and high  $Z_{SD}$  were found in the summer months. Increased chlorophyll and pheophytin (S2) in Cape Cod Bay during the winter months were consistent with the seasonal  $Z_{SD}$  trends observed. Opposite from seasonal variations in Buzzards Bay and Cape Cod Bay, Narragansett Bay  $Z_{SD}$  increased during the winter months and decreased during the summer months. Decreased chlorophyll, pheophytin, and total suspended solids measurements (S3) during the winter months were consistent with the Narragansett Bay seasonal in situ and L8  $Z_{SD}$  trends.



Fig. 4. Time series plots (2013–2017) of in situ and L8  $Z_{SD}$  A) Boston Harbor Site 142 B) Buzzards Bay Central Buzzards Bay Buoy Site C) Cape Cod Bay Site 6S D) Upper Narragansett Bay Bullock's Reach Buoy site.

3.4.  $Z_{SD}$  spatial assessment

Based on the acceptable same-day validation (see Fig. 2), L8  $Z_{SD}$  maps were generated for Buzzards Bay (Fig. 5), Cape Cod Bay (Fig. 6), and Narragansett Bay (Fig. 7) for a single day, March 14, 2014. While the  $Z_{SD}$  maps are a snapshot of the water clarity conditions during the time of L8 overpass, the maps illustrate regional spatial patterns. For Buzzards Bay (Fig. 5a), there were distinct differences in  $Z_{SD}$  between the individual embayments and between the embayments and central Buzzards Bay; the embayments bordering southeastern mainland Massachusetts appeared to have lower  $Z_{SD}$  than the embayments bordering the western edge of Cape Cod, Central Buzzards Bay, and Vineyard Sound. Cape Cod Bay  $Z_{SD}$  patterns differed from Buzzards Bay where low  $Z_{SD}$  spanned from offshore to inshore (Fig. 6a). Low  $Z_{SD}$  were observed nearshore and narrow bands of low  $Z_{SD}$  appeared to extend into

the middle of Cape Cod Bay. Lastly, low  $Z_{SD}$  (1.5–3.5 m) appeared to be uniformly spread across Upper Narragansett Bay with no distinctive  $Z_{SD}$  differences between Upper Narragansett Bay's inlets and the center of Upper Narragansett Bay (Fig. 7a).

In Fig. 5b, Transect A extends 11 km from a New Bedford Harbor sampling station to the central Buzzards Bay buoy station.  $Z_{SD}$  generally oscillated between 4 and 6 m along Transect A and roughly meter scale  $Z_{SD}$  variations are observed between pixels. Transect B extends 25 km from Manomet Bay station to the central Buzzards Bay buoy station where the  $Z_{SD}$  increased from 3.5 to 6 m for the first 15 km and then oscillated between 4 and 6 m (Fig. 5c). For Fig. 6b, Cape Cod Bay's Transect A extends for 35 km from sites 5 N (offshore Long Point, MA) to 9S (offshore of Ellenville, MA) where  $Z_{SD}$  (5–6 m) was observed in the first third of transect before increasing to 7 m. Dynamic  $Z_{SD}$  variations occurred in the latter part of the transect where the transect transitions

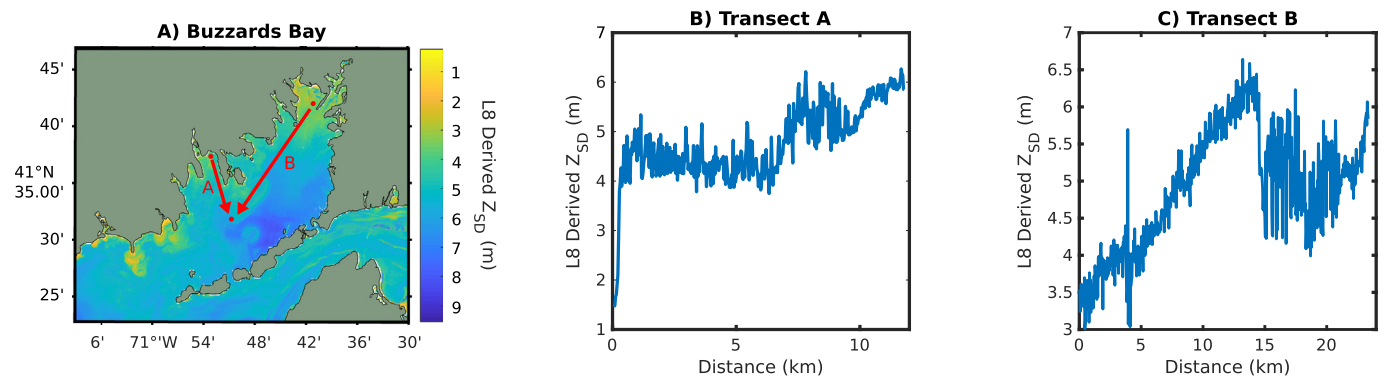


Fig. 5. A) L8  $Z_{SD}$  map of Buzzards Bay B) Transect between Potter's Cove and Central Buzzards Bay sites C) Transect between Manomet Bay and Central Buzzards Bay sites.

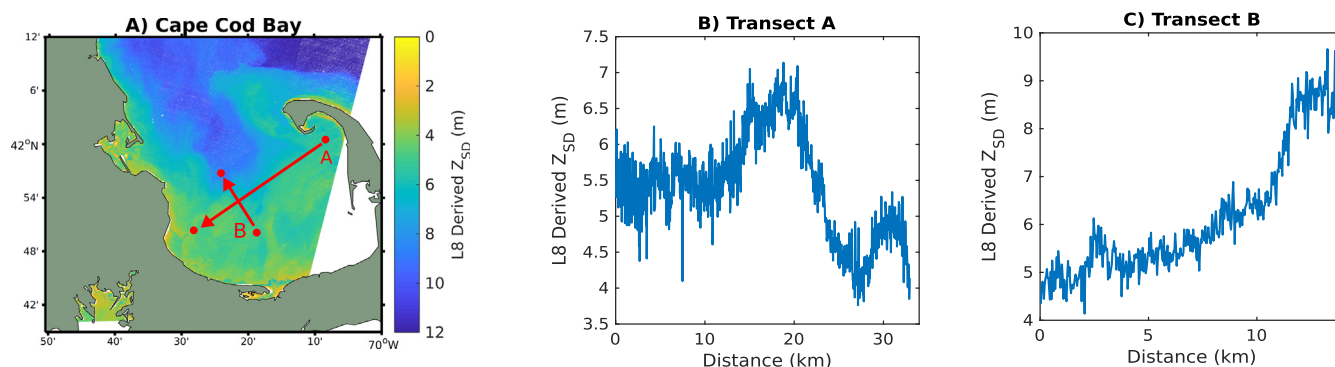


Fig. 6. A) L8  $Z_{SD}$  map of Cape Cod Bay B) Transect between sites 7S and 8 M C) Transect between sites 5N and 9S.

from the center of Cape Cod Bay to offshore Ellissville, MA. Transect B extends 15 km from sites 8 M to 7S where  $Z_{SD}$  increased along the transect from 4.5 to 9.5 m (Fig. 6c).

For Fig. 7b, the Narragansett Bay transect extends from the Edgewood Yacht Club station to the Bullock Reach station (5 km).  $Z_{SD}$  ranged between 1.5 and 3.5 m between the two stations, and the gap in the transect is where the transect is laid over land. As in Figs. 5 and 6,  $Z_{SD}$  measurements between pixels varied roughly on the scale of a meter; however, no  $Z_{SD}$  trends are observed between the stations.

#### 4. Discussion

##### 4.1. Same-day in situ $Z_{SD}$ and L8 $Z_{SD}$

The good agreement between in situ and L8  $Z_{SD}$  for same day matchups at Buzzards Bay, Cape Cod Bay, and Narragansett Bay (Fig. 2) was likely related to the L8  $Z_{SD}$  algorithm's semi-analytical basis. The L8  $Z_{SD}$  algorithm used  $R_{rs}$  information from all L8 visible bands (443, 481, 554, 656 nm) and depended on the derivation of  $a$  and  $b_b$  from the Quasi-Analytical Algorithm and the semi-analytical nature of  $K_d$  (Lee et al., 2016). The semi-analytical estimation of inherent and apparent optical properties allows for the application of the L8  $Z_{SD}$  algorithm to a range of coastal environments. Additionally, this assessment highlighted the potential to derive and validate other water quality parameters such as turbidity and suspended particulate matter following mechanistic approaches.

The differences between in situ and L8  $Z_{SD}$  were likely related to atmospheric correction methods, QAA accuracy, and spatial variation in water clarity. Ideally, measurements of in situ  $R_{rs}$  values would be compared with the L8  $R_{rs}$  output to gauge the accuracy of SeaDAS's atmospheric correction parameters (Wei et al., 2018); however, since

this validation solely depended on in situ  $Z_{SD}$ , it was best to process the L8 images with SeaDAS default conditions. Also, without in situ measurements of  $R_{rs}$ ,  $a$ , and  $b_b$ , we were not able to propagate the uncertainties associated with each QAA step like in Rodriguez et al. (2017). While the Buzzards Bay, Cape Cod Bay, and Narragansett Bay results were acceptable for this study, coinciding in situ  $R_{rs}$ ,  $a$ , and  $b_b$  measurements are necessary to determine which L8  $Z_{SD}$  algorithm steps limit the accuracy of the  $Z_{SD}$  retrieval. Propagating the uncertainties along each step of the L8  $Z_{SD}$  algorithm is necessary for determining if the SeaDAS atmospheric correction parameters need to be adjusted, if the derivation of IOPs with QAA needs to be reevaluated, or if a sensor with a higher spatial resolution is required. Negative biases for L8's blue and green bands were observed for Boston Harbor's  $R_{rs}$  validation (Wei et al., 2018), which may explain the overestimation of Boston Harbor L8  $Z_{SD}$  in this study. However, a follow up assessment with in situ optical instrumentation would be required to link the L8  $Z_{SD}$  overestimation with L8  $R_{rs}$  quality. It is important to reiterate that the in situ optical instrumentation required to investigate the limitations of the L8  $Z_{SD}$  algorithm is expensive and the accompanying field work and data processing is laborious, which would be especially burdensome on water quality monitoring groups.

Without in situ optical measurements, water quality monitoring organizations can evaluate local tidal cycles, assess proximity of sampling stations to land, and account for local boating activity to constrain the validation and application of the L8  $Z_{SD}$  algorithm. When the effects of daily tidal cycles are minimized by limiting the validation to a three-hour window, the RMSE, MAPD, and  $R^2$  improved slightly, but the results do not provide confidence in the L8  $Z_{SD}$  retrieval in Boston Harbor ( $N = 20$ , RMSE = 1.3 m, MAPD = 50%,  $R^2 = 0.11$ ). The poor results were further examined by assessing the proximity of sampling stations to land. Surface reflectance from land can impact the quality of

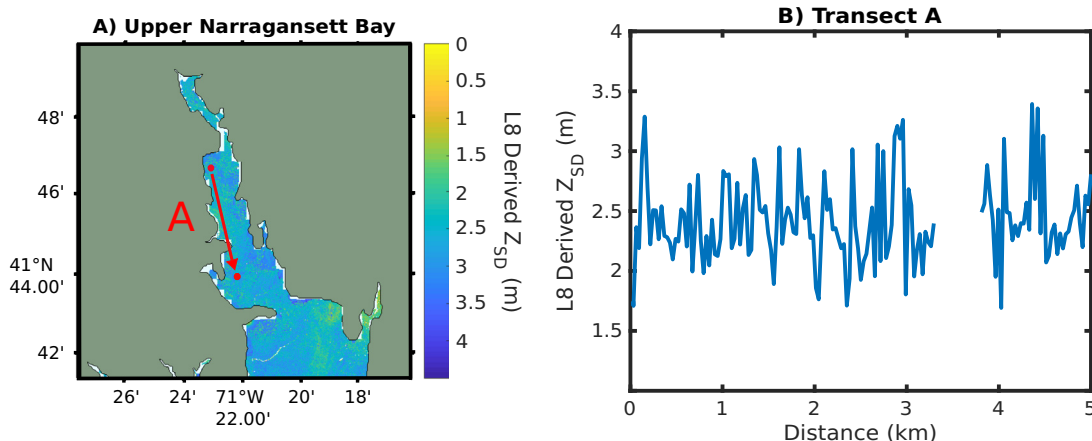


Fig. 7. A) L8  $Z_{SD}$  map of Upper Narragansett Bay B) Transect between Edgewood Yacht Club and Bullock's Reach Buoy sites.

L8  $R_{rs}$  because the radiance reflected from land can be scattered by the atmosphere into the field of view of nearshore stations, also known as adjacency effects (Bulgarelli et al., 2014). Removing nearshore stations slightly improved the statistics ( $N = 9$ ,  $RMSE = 1.26$  m,  $MAPD = 45\%$ ,  $R^2 = 0.14$ ); however, the results do not provide confidence in the application of the L8  $Z_{SD}$  algorithm to Boston Harbor. Lastly, Boston Harbor is the largest seaport in New England with active ports, numerous shipping lanes, and high recreational boating activity. Boat wakes and mixing from high boating activity can impact L8's  $R_{rs}$  quality; thus, a broader investigation into L8  $R_{rs}$  spatial variations in urban harbors is required to resolve these concerns.

Local biogeochemical information can also be used to confine the temporal window used for the L8  $Z_{SD}$  validation. The degree of autocorrelation from high frequency measurements of optically variable constituents provides information about the temporal variability of water clarity. To demonstrate this concept, we looked at Narragansett Bay's Bullock's Reach station where an in situ fluorometer measures chlorophyll every 15 min. The temporal window was expanded to the time point where chlorophyll became decorrelated, and the increased number of matchups were still in good agreement ( $N = 35$ ,  $RMSE = 0.69$  m,  $MAPD = 34\%$ ,  $R^2 = 0.08$ ). It is important to reiterate that the combination of optically variable constituents (i.e. phytoplankton, colored dissolved organic matter, detritus) determines water clarity and as a result, chlorophyll measurements alone will not precisely capture the temporal variation in water clarity. Nevertheless, this work demonstrates how high frequency biogeochemical information can systematically confine the temporal validation window of the L8  $Z_{SD}$  algorithm and other remote sensing water quality algorithms.

#### 4.2. $Z_{SD}$ range and distribution variability

The  $Z_{SD}$  range and distribution variability assessment evaluated the performance of the L8  $Z_{SD}$  algorithm across all 58 images. The histogram and box-whisker plot comparison in Fig. 3 demonstrates how L8  $Z_{SD}$  throughout 2013–2017 generally captured the  $Z_{SD}$  range and distribution variability observed across Boston Harbor, Buzzards Bay, Cape Cod Bay, and Narragansett Bay. Since in situ  $Z_{SD}$  were only selected if a sampling station fell within an atmospherically corrected L8 pixel and if the in situ  $Z_{SD}$  occurred in the same month and year of an L8 image, the comparison will at best capture seasonal variations.

#### 4.3. $Z_{SD}$ temporal validation

In general, L8's short operational lifetime up to this point (2013–2018), 16-day repeat orbit, and coastal Massachusetts' regularly cloudy conditions limited the L8  $Z_{SD}$  retrievals across all seasons (Fig. 4). Despite the temporal sampling difficulties, spatio-temporal information could still be gleaned. For site 142 in Boston Harbor, seasonal trends were not observed across in situ and L8  $Z_{SD}$ . At the intersection of Boston Harbor's President Road's channel and the Broad North and South Channels, site 142 may not have observable seasonal trends because of mixing and surface wakes from high boating activity. On the other hand, Bullock's Reach station in Narragansett Bay displayed distinct seasonal patterns where higher  $Z_{SD}$  were found during the winter months than in the summer months. Low  $Z_{SD}$  is most likely related to warming temperatures and nutrient loading increasing phytoplankton abundance, which is consistent with observations from local monitoring groups (Borkman and Smayda, 1998).

The seasonal  $Z_{SD}$  trend in Narragansett Bay was reversed in Cape Cod Bay, where in situ and L8  $Z_{SD}$  at site 9S were low during the winter and spring months. Increased in situ chlorophyll and pheophytin data during the winter indicated  $Z_{SD}$  was primarily influenced by seasonal changes in phytoplankton abundance. Existing research further supports low winter and spring L8  $Z_{SD}$  observations where Cape Cod Bay's well mixed conditions trigger a phytoplankton bloom that is terminated in the late spring and early summer due to temperature induced water

column stratification (Keller et al., 2001; Kelly and Doering, 1997). This seasonal pattern leads to lower water clarity during the early spring and higher water clarity at the onset of late spring and early summer.

Lastly, L8  $Z_{SD}$  in Buzzards Bay exhibited a similar trend to Cape Cod Bay where low  $Z_{SD}$  was observed across all three years in the winter months. While increases in nitrate and nitrite have been observed after increased diatom abundance in the winter (Turner et al., 2009), without accompanying in situ water chemistry and optical information we were not able to verify a seasonal pattern in Buzzards Bay. A long-term assessment of in situ  $Z_{SD}$  and accompanying water chemistry data is necessary to determine a seasonal trend in  $Z_{SD}$ .

#### 4.4. L8 $Z_{SD}$ water clarity maps-spatial assessment

The L8  $Z_{SD}$  algorithm was applied to an example single-day image from March 14, 2014 and water clarity maps were generated for Buzzards Bay, Cape Cod Bay, and Narragansett Bay (Figs. 5, 6, and 7) because of the acceptable same-day in situ and L8  $Z_{SD}$  validation (Fig. 2). The Buzzards Bay  $Z_{SD}$  map in Fig. 5a exhibited distinct inshore and offshore water clarity patterns, likely related to the dilution of optically variable water constituents with depth and distance from shore-based nutrient sources. For Cape Cod Bay's  $Z_{SD}$  map in Fig. 6a, low  $Z_{SD}$  spatial patterns were found inshore and offshore. The L8  $Z_{SD}$  variations specifically observed on the western edge of Cape Cod Bay could be linked to the counter-clockwise circulation of Massachusetts Bay, tidal fluxes, timing of the spring phytoplankton bloom, inland nutrient discharge, or a combination of the above. Unlike Buzzards Bay and Cape Cod Bay, low  $Z_{SD}$  was uniform across Upper Narragansett Bay (1.5–3.5 m). Upon closer inspection of the L8  $Z_{SD}$  map, Upper Narragansett Bay water clarity conditions were relatively patchy, which could be related to minor variations in  $Z_{SD}$  (i.e.  $\Delta Z_{SD} < 1$  m) being highlighted, L8's 30 m spatial resolution not capturing water clarity patterns at smaller spatial scales, or a combination of the above.

Water quality monitoring groups can use L8  $Z_{SD}$  maps, in situ  $Z_{SD}$ , water chemistry information, bathymetry, and storm information to investigate the drivers of water clarity patterns and determine the geographical origin of low water clarity patterns. It is important to note that nearshore L8  $Z_{SD}$  will need to be interpreted with caution due to adjacency effects from land and bottom reflectance effects on the retrieval of L8  $R_{rs}$ . Parameterizing the L8  $Z_{SD}$  algorithm for shallow and deep waters is beyond the scope of this work and bottom reflectance concerns nearshore can be addressed by using existing in situ or satellite bathymetry datasets to filter L8 pixels susceptible to bottom reflectance effects.

The  $Z_{SD}$  transects in Figs. 5, 6, and 7 capture water clarity variability between Buzzards Bay, Cape Cod Bay, and Narragansett Bay point sampling stations and provide a visualization of the high spatial  $Z_{SD}$  variation between sampling stations. The spatial variability between point stations will be characterized with a structure function analysis in future work. The combination of L8 maps and transects were presented to demonstrate how water quality monitoring groups can use L8  $Z_{SD}$  information to inform their sampling efforts. For example, water quality monitoring groups could use L8  $Z_{SD}$  maps and transects to expand their sampling efforts to other locations in their region of interest. Lastly, L8  $Z_{SD}$  transects and maps can be further evaluated with structure functions (i.e. variograms) to quantify L8 sensor noise, QAA, and L8  $Z_{SD}$  algorithm error, and to further understand spatial patterns across Buzzards Bay, Cape Cod Bay, and Narragansett Bay. Moving forward, some of the limitations of L8 imagery, moderate 30 m resolution and 16-day repeat coverage, can be addressed by supplementing with additional remote sensing imagery from targeted meter and sub-meter resolution airborne drone surveys, and potentially high-resolution commercial satellites.

## 5. Summary

The in situ and L8 Z<sub>SD</sub> same-day validation, range, variability, temporal, and spatial water clarity assessments provided confidence in the application of L8 Z<sub>SD</sub> algorithm to Buzzards Bay, Cape Cod Bay, Narragansett Bay. Geophysical and biogeochemical information from water quality monitoring organizations was used to inform the validation and application of the L8 Z<sub>SD</sub> algorithm. The application of the L8 Z<sub>SD</sub> algorithm ultimately prompts a more rigorous assessment of water clarity patterns from L8 Z<sub>SD</sub> maps and transects. In addition, extending this water clarity analysis to the entire Landsat archive and parameterizing the Lee et al. (2015) Z<sub>SD</sub> algorithm for the ESA Sentinel-2 MultiSpectral Instrument (MSI) will increase temporal coverage of water clarity and will improve our understanding of long-term water clarity change in Boston Harbor, Buzzards Bay, Cape Cod Bay, and Narragansett Bay. Pairing L8 Z<sub>SD</sub> measurements and maps with local water quality monitoring information will enhance water quality monitoring groups' efforts and, ultimately, better inform coastal managers, policy-makers, and communities about dynamic changes in coastal water clarity.

Supplementary data to this article can be found online at <https://doi.org/10.1016/j.marpolbul.2019.04.078>.

## Acknowledgements

This work was supported by the John D. and Catherine T. MacArthur Foundation (grant 14-106159-000-CFP) and by the National Science Foundation grant DGE 1249946, Integrative Graduate Education and Research Traineeship (IGERT): Coasts and Communities – Natural and Human Systems in Urbanizing Environments. Lastly, we are indebted to the Massachusetts Water Resources Authority, Buzzards Bay Coalition, Provincetown Center for Coastal Studies, Narragansett Bay Commission, and the numerous citizen scientists responsible for collecting the in situ measurements used in this study. Comments and suggestions from our anonymous reviewer were greatly appreciated.

## References

- Aas, E., Høkedal, J., Sørensen, K., 2014. Secchi depth in the Oslofjord-Skagerrak area: theory, experiments and relationships to other quantities. *Ocean Sci.* 10 (2), 177–199. <https://doi.org/10.5194/os-10-177-2014>.
- Barnes, B.B., Hu, C., Hølekamp, K.L., Blonski, S., Spiering, B.A., Palandro, D., Lapointe, B., 2014. Use of Landsat data to track historical water quality changes in Florida Keys marine environments. *Remote Sens. Environ.* 140, 485–496. <https://doi.org/10.1016/j.rse.2013.09.020>.
- Borkman, D.G., Smayda, T.J., 1998. Long-term trends in water clarity revealed by Secchi-disk measurements in lower Narragansett Bay. *ICES J. Mar. Sci.* 55 (4), 668–679. <https://doi.org/10.1006/jmsc.1998.0380>.
- Boyce, D.G., Lewis, M., Worm, B., 2012. Integrating global chlorophyll data from 1890 to 2010. *Limnol. Oceanogr. Methods* 10 (11), 840–852. <https://doi.org/10.4319/lom.2012.10.840>.
- Bulgarelli, B., Kiselev, V., Zibordi, G., 2014. Simulation and analysis of adjacency effects in coastal waters: a case study. *Appl. Opt.* 53 (8), 1523. <https://doi.org/10.1364/AO.53.001523>.
- Chen, Z., Muller-Karger, F.E., Hu, C., 2007. Remote sensing of water clarity in Tampa Bay. *Remote Sens. Environ.* 109 (2), 249–259. <https://doi.org/10.1016/j.rse.2007.01.002>.
- Crooke, B., McKinna, L.L.W., Cetinić, I., 2017. From toes to top-of-atmosphere: Fowler's Sneaker Depth index of water clarity for the Chesapeake Bay. *Opt. Express* 25 (8), A361. <https://doi.org/10.1364/OE.25.00A361>.
- Doron, M., Babin, M., Mangin, A., Hembise, O., 2007. Estimation of light penetration, and horizontal and vertical visibility in oceanic and coastal waters from surface reflectance. *J. Geophys. Res. Oceans* 112 (6), C06003. <https://doi.org/10.1029/2006JC004007>.
- Doron, M., Babin, M., Hembise, O., Mangin, A., Garnesson, P., 2011. Ocean transparency from space: validation of algorithms estimating Secchi depth using MERIS, MODIS and SeaWiFS data. *Remote Sens. Environ.* 115 (12), 2986–3001. <https://doi.org/10.1016/j.rse.2011.05.019>.
- Duntley, S.Q., Preisendorfer, R.W., 1952. The Visibility of Submerged Objects.
- Hellweger, F.L., Schlosser, P., Lall, U., Weisell, J.K., 2004. Use of satellite imagery for water quality studies in New York Harbor. *Estuar. Coast. Shelf Sci.* 61 (3), 437–448. <https://doi.org/10.1016/j.ecss.2004.06.019>.
- Keller, A.A., Taylor, C., Oviatt, C., Dorrington, T., Holcombe, G., Reed, L., 2001. Phytoplankton production patterns in Massachusetts Bay and the absence of the 1998 winter-spring bloom. *Mar. Biol.* 138 (5), 1051–1062. <https://doi.org/10.1007/s002270000525>.
- Kelly, J.R., Doering, P.H., 1997. Monitoring and modeling primary production in coastal waters: studies in Massachusetts Bay 1992–1994. In: *Marine Ecology Progress Series*. Inter-Research Science Center. <https://doi.org/10.2307/24857481>.
- Kloiber, S.M., Brezonik, P.L., Olmanson, L.G., Bauer, M.E., 2002. A procedure for regional lake water clarity assessment using Landsat multispectral data. *Remote Sens. Environ.* 82 (1), 38–47. [https://doi.org/10.1016/S0034-4257\(02\)00022-6](https://doi.org/10.1016/S0034-4257(02)00022-6).
- Lee, Z., Carder, K.L., Arnone, R.A., 2002. Deriving inherent optical properties from water color: a multiband quasi-analytical algorithm for optically deep waters. *Appl. Opt.* 41 (27), 5755. <https://doi.org/10.1364/AO.41.005755>.
- Lee, Z., Du, K.P., Arnone, R., 2005. A model for the diffuse attenuation coefficient of downwelling irradiance. *J. Geophys. Res. C: Oceans* 110 (2), 1–10. <https://doi.org/10.1029/2004JC002275>.
- Lee, Z., Hu, C., Shang, S., Du, K., Lewis, M., Arnone, R., Brewin, R., 2013. Penetration of UV-visible solar radiation in the global oceans: insights from ocean color remote sensing. *J. Geophys. Res. Oceans* 118 (9), 4241–4255. <https://doi.org/10.1002/jgrc.20308>.
- Lee, Z., Shang, S., Hu, C., Du, K., Weidemann, A., Hou, W., ... Lin, G., 2015. Secchi disk depth: a new theory and mechanistic model for underwater visibility. *Remote Sens. Environ.* 169, 139–149. <https://doi.org/10.1016/j.rse.2015.08.002>.
- Lee, Z., Shang, S., Qi, L., Yan, J., Lin, G., 2016. A semi-analytical scheme to estimate Secchi-disk depth from Landsat-8 measurements. *Remote Sens. Environ.* 177, 101–106. <https://doi.org/10.1016/j.rse.2016.02.033>.
- Lim, J., Choi, M., 2015. Assessment of water quality based on Landsat 8 operational land imager associated with human activities in Korea. *Environ. Monit. Assess.* 187 (6), 384. <https://doi.org/10.1007/s10661-015-4616-1>.
- Olmanson, L.G., Brezonik, P.L., Finlay, J.C., Bauer, M.E., 2016. Comparison of Landsat 8 and Landsat 7 for regional measurements of CDOM and water clarity in lakes. *Remote Sens. Environ.* 185, 119–128. <https://doi.org/10.1016/j.rse.2016.01.007>.
- Preisendorfer, R.W., 1986. Secchi disk science: visual optics of natural waters. *Limnol. Oceanogr.* 31 (5), 909–926. <https://doi.org/10.4319/lo.1986.31.5.0909>.
- Rodrigues, T., Alcântara, E., Watanabe, F., Imai, N., 2017. Retrieval of Secchi disk depth from a reservoir using a semi-analytical scheme. *Remote Sens. Environ.* 198, 213–228. <https://doi.org/10.1016/j.rse.2017.06.018>.
- Sun, D., Hu, C., Qiu, Z., Shi, K., 2015. Estimating phycocyanin pigment concentration in productive inland waters using Landsat measurements: a case study in Lake Dianchi. *Opt. Express* 23 (3), 3055. <https://doi.org/10.1364/OE.23.003055>.
- Trinh, R.C., Fichot, C.G., Gierach, M.M., Holt, B., Malakar, N.K., Hulley, G., Smith, J., 2017. Application of Landsat 8 for monitoring impacts of wastewater discharge on coastal water quality. *Front. Mar. Sci.* 4, 329. <https://doi.org/10.3389/fmars.2017.00329>.
- Turner, J., Borkman, D., Lincoln, J., Gauthier, D., Petitpas, C., 2009. *Plankton studies in Buzzards Bay, Massachusetts, USA. VI. Phytoplankton and water quality, 1987 to 1998.* *Mar. Ecol. Prog. Ser.* 376, 103–122.
- Weeks, S., Werdell, P.J., Schaffelke, B., Canto, M., Lee, Z., Wilding, J.G., Feldman, G.C., 2012. Satellite-derived photic depth on the great barrier reef: spatio-temporal patterns of water clarity. *Remote Sens.* 4 (12), 3781–3795. <https://doi.org/10.3390/rs4123781>.
- Wei, J., Lee, Z., Garcia, R., Zoffoli, L., Armstrong, R.A., Shang, Z., Chen, R.F., 2018. An assessment of Landsat-8 atmospheric correction schemes and remote sensing reflectance products in coral reefs and coastal turbid waters. *Remote Sens. Environ.* 215, 18–32. <https://doi.org/10.1016/j.rse.2018.05.033>.
- Wernand, M.R., 2010. On the history of the Secchi disc. *J. Eur. Opt. Soc.* 5 (0), 10013s. <https://doi.org/10.2971/jeos.2010.10013s>.